https://doi.org/10.5194/egusphere-2022-60
Preprint. Discussion started: 25 April 2022

Improving continuous-flow analysis of triple oxygen isotopes in ice cores: insights from replicate measurements

Lindsey Davidge[1], Eric J. Steig[1], Andrew J. Schauer[1]

[1]Department of Earth and Space Science, University of Washington, Seattle, 98195, USA

Correspondence to: Lindsey Davidge (ldavidge@uw.edu)

Abstract. Stable water isotope measurements from polar ice cores provide high-resolution information about past hydrologic conditions and are therefore important to understanding Earth's climate system. Routine high-resolution measurements of $\delta^{18}O$, δD, and deuterium excess are made by continuous-flow analysis (CFA) methods that include laser spectroscopy instruments. Recent advances in instrumentation allow for simultaneous measurements of all stable water isotopes, including $\delta^{17}O$ and ^{17}O excess ($\Delta^{17}O$). Here, we present replicate measurements of an ice core sample taken from Summit, Greenland, using a CFA system coupled to a cavity ring-down laser spectroscopy (CRDS) instrument. We demonstrate that our CFA-CRDS method can make high-precision measurements of $\Delta^{17}O$ (<5 per meg) with high resolution (a few cm) in ice core samples. We find that calibration errors generate most of the variability among the replicate datasets. Our work shows that CFA-CRDS methods can detect seasonal variability in $\Delta^{17}O$. We suggest that CFA-CRDS methods should be applied to ice core measurements when high-resolution information is desired.

1 Introduction

Records of water isotopologues from ice cores are fundamental to the study of past climate processes (Dansgaard, 1964). Oxygen ($\delta^{18}O$) and hydrogen (δD) isotope ratios have been measured routinely in ice-core samples and in other natural waters due to their well understood, first-order equilibrium fractionation relationship to atmospheric temperature (Jouzel et al., 1997). Additionally, deuterium excess (d) is commonly used as an indicator of kinetic fractionation processes within the hydrologic cycle (Merlivat and Jouzel, 1979). Deuterium excess is conventionally defined as:

$$d = \delta D - 8 * \delta^{18}O. \quad (1)$$

Barkan and Luz (2005) showed that measuring $\delta^{17}O$ and $\delta^{18}O$ at sufficiently high precision allows for the determination of ^{17}O excess ($\Delta^{17}O$), a quantity that, like d, also reflects nonequilibrium fractionation processes such as sea-surface humidity (Uemera et al., 2010) and supersaturation effects during snow formation (Schoenemann et al., 2014). $\Delta^{17}O$ is defined by Luz and Barkan (2010) as the deviation in $\delta^{17}O$ from the global meteoric water line:

$$\Delta^{17}O = \ln(\delta^{17}O + 1) - 0.528 \ln(\delta^{18}O + 1), \quad (2)$$

https://doi.org/10.5194/egusphere-2022-60
Preprint. Discussion started: 25 April 2022

where δ ("delta") values are expressed as a unitless fractional deviation from Vienna Standard Mean Ocean Water (VSMOW; see e.g., Schoenemann et al., 2013, for a complete discussion of nomenclature).

Measurements of $\delta^{18}O$, δD, and *d* by laser spectroscopy are routine in many laboratories (e.g., Kerstel et al., 1999; Iannone, 2010; Steen-Larsen, 2014; Schauer et al., 2016; Jones et al., 2017). For water-isotope measurements of ice cores, it is increasingly common to couple a laser spectroscopy instrument with a continuous-flow analysis (CFA) system. CFA processing reduces sample handling and can produce very high depth-resolution (originally described by Gkinis et al., 2010; 2011). Highly resolved water isotope measurements are advantageous for a variety of studies, such as those that use the water-isotope diffusion length to infer information about firn processes or to reconstruct temperature histories (e.g., Gkinis et al., 2014; Kahle et al., 2018; 2021; Jones et al, 2017b). It is desirable to obtain measurements of $\delta^{17}O$ and $\Delta^{17}O$ at a resolution comparable to that for $\delta^{18}O$, δD, and *d*. Corresponding measurements of both $\Delta^{17}O$ and *d* – which have differing sensitivities to kinetic fractionation processes – could help to disentangle the various processes that influence water isotope values during evaporation, atmospheric transportation and snow formation (Angert et al., 2004; Uemera et al., 2010). However, measurements of $\Delta^{17}O$ require much higher precision than the other water-isotope ratios and have therefore generally been obtained by isotope-ratio mass spectrometry (IRMS) (Luz and Barkan, 2010; Landais et al., 2008; 2012; Schoenemann et al., 2013, 2014). Because the IRMS method is relatively expensive and time-consuming, $\Delta^{17}O$ measurements from ice cores are limited in spatial and temporal resolution (e.g., Landais et al., 2008; Schoenemann et al., 2014; Aron et al., 2021). CFA for $\Delta^{17}O$ has the potential to address this limitation.

Laser spectroscopy enables simultaneous measurements of $\delta^{17}O$, $\delta^{18}O$, and δD (and therefore *d* and $\Delta^{17}O$). Steig et al. (2014) developed a cavity-ring-down laser spectroscopy (CRDS) instrument for $\Delta^{17}O$ analysis, sold commercially as the Picarro L2140-*i*; other instruments with different spectroscopic methods have also been developed for $\Delta^{17}O$ analysis (e.g., Berman et al., 2013; Tian et al., 2016). Schauer et al. (2016) demonstrated that the L2140-*i* CRDS configured with an autosampler can routinely measure $\Delta^{17}O$ from discrete water samples with precision and accuracy comparable to IRMS methods. Steig et al. (2021) obtained continuous measurements of all water isotope quantities ($\delta^{17}O$, $\delta^{18}O$, δD, d, $\Delta^{17}O$) on an ice core from the South Pole by using the L2140-*i* CRDS coupled to the CFA system developed by Jones et al. (2017). However, despite the potential shown by these studies, the adoption of CFA-CRDS for $\Delta^{17}O$ faces two primary challenges. First, the integration time required for high-precision $\Delta^{17}O$ measurements by CRDS – approximately 1000 s to achieve precision of 10 per meg (Steig et al., 2014) – is much greater than the integration time required to achieve meaningful precision for $\delta^{18}O$, δD or *d*. Second, the CFA system – i.e., the melting and vaporization process used to introduce an ice-core sample into the CRDS – may further degrade the measurement quality by processes that are not yet well understood. For example, Steig et al. (2021) identified occasional large (>20 per meg) offsets in CFA-CRDS $\Delta^{17}O$ in their measurements of the South Pole ice core; the cause of these offsets was unclear. It is our goal to investigate the reproducibility of $\Delta^{17}O$ measurements of ice cores by CFA-CRDS.

https://doi.org/10.5194/egusphere-2022-60
Preprint. Discussion started: 25 April 2022

Here, we describe a CFA-CRDS measurement methodology that was designed for high-resolution measurements of $\Delta^{17}O$. We take advantage of archived ice-core samples from Summit, Greenland to make repeated CFA-CRDS measurements of $\Delta^{17}O$. These samples (collected by Hastings et al., 2009) provide an opportunity to more fully explore the potential and limitations of $\Delta^{17}O$ measurements by CFA-CRDS. We use replicate measurements made by CFA-CRDS and discrete CRDS methods to assess the relationship between precision and resolution of CFA-CRDS $\Delta^{17}O$ data and to identify sources of measurement error.

2 Methods

We use a CFA processing line in combination with a Picarro L2140-*i* laser spectrometer (Steig et al., 2014) to measure $\Delta^{17}O$ of ice core samples. The function of the CFA line is to generate a continuous supply of constant-humidity sample vapor to the CRDS analyzer. A constant stream of vaporized sample is important because errors in isotope-ratio measurements can arise from inconsistent sample pressure at the CRDS inlet (Gkinis et al., 2011; Schauer et al., 2016). We also aim to reduce diffusion and mixing within the CFA system to avoid smoothing the resulting record of $\Delta^{17}O$. We operate the CFA-CRDS system to measure nine repeated sections of ice core, in addition to a repeated sequence of internal reference waters that are used to calibrate the ice core measurements. For comparison, we also measure a tenth ice-core replicate by discrete CRDS.

2.1 CFA-CRDS design goals and custom vaporizer design

Continuous and complete vaporization is critical to reducing errors in all CRDS stable water isotope measurements, and it is especially important for attaining the per-meg precision necessary to detect meaningful variations in $\Delta^{17}O$. Previous studies have achieved continuous vaporization by heating sample water in the presence of dry air, either within an insulated stainless-steel tee (e.g., Gkinis et al., 2010; 2011) or within a concentric glass nebulizer with a vaporizing tube (e.g., Emanuelsson et al., 2015; Jones et al., 2017). Gkinis et al. (2010; 2011) designed a flash vaporization process to instantaneously vaporize a continuous stream of sample droplets; the flash vaporization process involves a continuous stream of liquid sample that is combined with a continuous stream of dry air inside a 0.50-mm internal diameter stainless-steel tee at near-ambient pressure. Steig et al. (2021) measured $\Delta^{17}O$ by CFA-CRDS with the CFA configuration of Jones et al. (2017): a continuous stream of water sample at 1030 kPa (150 psi) is aerosolized within a concentric glass nebulizer; the aerosolized sample droplets then evaporate completely within a 1.8-cm internal diameter, 20-cm-long glass vaporizing tube that is heated to 200° C. In this configuration, the CRDS analyzer draws vaporized sample from the vaporizing tube, and excess sample vapor is vented to laboratory air. Two critical differences between the Gkinis et al. (2010; 2011) and Jones et al. (2017) methods are the volume of the vaporization chamber and the volume of vapor that is generated. The smaller volume of the flash vaporizer should limit signal smoothing between the vaporizer and the analyzer. However, the flash vaporization method described by Gkinis (2010; 2011) generates vapor at approximately the rate that it is required by the analyzer, whereas the nebulizer method of Jones

https://doi.org/10.5194/egusphere-2022-60
Preprint. Discussion started: 25 April 2022

(2017) produces an excess of vapor that is vented prior to reaching the analyzer. Producing excess vapor is another way to limit the signal smoothing upstream of the vapor vent because it increases the velocity of sample through the system.

For this study, we built a custom vaporizer unit that benefits from both the small volume of the flash vaporizer and also the production of excess sample vapor. We use a 0.50-mm stainless-steel tee as used by Gkinis et al. (2010; 2011), but we operate our vaporizer at a much higher mixing pressure (typically 200 kPa) than is used by Gkinis et al. to produce and vent several times more vapor than is required for analysis. A small system volume combined with a high volumetric flow rate leads to a short retention time within the vaporizer that limits mixing of adjacent ice core layers. An additional benefit of the small vaporizer volume is that flow inconsistencies (i.e., changes in sample flow rate caused by flow obstructions or bubble interruptions) that may occur within the vaporizer can be observed by the near-instantaneous analyzer output; patterns in water vapor concentration or instantaneous isotope readings provide information about vaporization conditions that is important for identifying and avoiding water isotope fractionation. We use instantaneous CRDS observations of water concentration and uncalibrated water isotope values to infer vaporization conditions that may affect $\Delta^{17}O$. We monitor flow conditions within the CFA system by incorporating electronic pressure sensors. Instantaneous instrument output that reflects the internal vaporizer conditions and monitoring of the CFA line pressures provide information that is used to tune the CFA-CRDS system during analysis, with the goal of reducing possible isotope fractionation that may cause errors in $\Delta^{17}O$.

2.2 CFA-CRDS system configuration

The CFA configuration is described in this section and shown in Fig. 1.

Glacial ice is melted on a 30-mm x 30-mm aluminium melt head that is fitted with four resistance heater cartridges and held at constant temperature by a PID controller (Bigler et al., 2011). Sample melt is drawn away from the melt head and through an automated selector valve (VICI, p/n C25Z-3186EMH) by a dedicated peristaltic pump, PUMP-1 (MasterFLex L/S 7535-04). The automated valve is configured to select a rotating sequence of calibration standards when ice cores are not being measured. Measured waters are carried by 0.5-mm internal diameter PFA conveyance tubing between all system components prior to the vaporizer. From PUMP-1, water flows through a Darwin Microfluidics gas-permeable membrane bubble trap (44µL internal volume, p/n LVF-3526) where bubbles are removed and vented to the laboratory air. Excess water is then vented and containerized. Water is drawn away from the vent by PUMP-2 (same model as PUMP-1), whose flow rate is set to match the demand of the downstream vaporizer, which is much smaller than the supply of melt water from the ice core. The vent accommodates the differences between PUMP-1 (which controls the melt rate) and PUMP-2 (which controls the vaporization rate). Water flows through 2-µm and 1-µm in-line filters in series to restrict the flow of particulates into the vaporizer. PUMP-2 is also preceded and followed by electronic pressure sensors PI-1 (Elveflow PS3-Small) and PI-2 (Elveflow PS4-Small) to monitor injection pressure conditions and pump and filter performance. Typically, the pressurized dry air entering the vaporizer adds backpressure on the liquid sample injection line, which damps the cyclic pressure

https://doi.org/10.5194/egusphere-2022-60
Preprint. Discussion started: 25 April 2022

fluctuations of the peristaltic pump and leads to more constant vaporizer operations; this allows us to balance the sample pressure with the pressure of the dry air line. The system also includes a flow valve (FV-1) that can also be used to adjust the backpressure on PUMP-2.

At the vaporizer, filtered sample water is mixed and heated with dry air to produce a constant-humidity stream of vaporized sample. Immediately before entering the vaporizer, the liquid sample line is reduced to a 100-µm fused silica capillary tube. The 100-µm capillary generates droplets small enough to vaporize instantaneously, but it also clogs less easily than capillary with a smaller diameter. The custom vaporizer includes a 0.50-mm internal diameter tee heated to 170°C using a PID-controlled resistance heater cartridge, similar to Gkinis et al. (2010; 2011). The vaporizer combines pressurized dry air with liquid sample, and it is set within an aluminium enclosure that is lined with 3.175 cm of calcium silicate insulation. After the sample is vaporized, excess vapor is vented into the laboratory to prevent pressure fluctuations within the analytical cavity; the required sample volume is drawn into the analyzer. The measured volume is carried from the vaporizer to the instrument cavity within insulated tubing to prevent condensation.

2.3 Reducing system memory

Because our automated selector valve is positioned immediately after the ice core melt head, reference waters pass through all system instrumentation and tubing except the melt head tubing itself; by design, the mixing length expected between measured ice core layers with differing isotopic composition can be approximated by the mixing length represented by transitions in reference waters, if all other system conditions are identical. Mixing length within the system is minimized in two ways: system instrumentation volume and system tubing diameter were minimized to limit the retention time of sample within the processing line, and excess sample volume is drawn through the entire system during CFA analysis to condition the processing line to the isotopic composition of the next incremental volume. During ice-core measurements, excess liquid volume is created by the differential between PUMP-1 and PUMP-2, and it is vented before PUMP-2. Excess vapor volume is created by the differential between PUMP-2 and the L2140-*i* inlet pump, and it is vented to laboratory air immediately before entering the analytical cavity. In this way, the liquid and vapor tubing is flushed with several times more sample volume than is required for analysis.

The transition time between reference waters is a conservative estimate of sample mixing within the CFA system because, during reference-water measurements, the pump rate at PUMP-1 is minimized to preserve reference water volume. During ice-core analysis, higher pump rates at PUMP-1 drive shorter retention times within the upstream system tubing and therefore reduce system mixing. Higher flow rates at PUMP-1 also causes a greater difference between pump rates that increases the conditioning volume that is vented before PUMP-2. During reference-water measurements, we expect much slower flow through the tubing and therefore expect longer transition times. The transition time between measurements of reference waters generally varied between 3 and 6 minutes. We therefore assume a conservative mixing time of 360 seconds during reference water transitions, and we ignore the 360 seconds that initiate and conclude each reference water measurement. We show typical

https://doi.org/10.5194/egusphere-2022-60
Preprint. Discussion started: 25 April 2022

reference water transition intervals in Fig. 2. Before measuring each section of ice (which is typically ~1 m long), we also condition the system with at least ten minutes of water with similar isotopic composition to prevent mixing between isotopically disparate reference waters and ice core samples at the beginning of the analysis. Finally, the duplicate CFA-CRDS measurements that are the focus of this study serve as a practical evaluation of the effects of memory on measurement fidelity in this configuration.

2.4 Operational considerations

Because the vaporizer is sensitive to small fluctuations in sample flow rate, a careful balance of system pressures is required to control sample flow (Gkinis et al., 2010; 2011); specifically, the pressure of the sample at the vaporizer inlet must be slightly greater than the pressure of the dry air within the vaporizer. We discuss system operations in the context of this pressure balance instead of using flow rates, since the flow rates during analysis depend on a complex network of component pressures that are continually evolving during analysis, e.g., by particulate loading at F-1 or F-2 or by precipitate accumulation within the vaporizer.

Maintaining a balance between the air pressure and sample pressure within the vaporizer requires knowledge of both pressure conditions. We monitor pressures at PI-1 and PI-2 so that it is possible to diagnose the source of system pressure changes when they occur; we also fix the pressure of the dry air line with the backpressure regulator (typically 200 kPa). Vacuum conditions at PI-1 indicate particulate loading across the filter screen at F-1; the filter screen will clog over time and, if the filter screen is not replaced, suction from the inlet of PUMP-1 can draw a vacuum at PI-1. Vacuum conditions at PI-1 can impact the downstream peristaltic pump (PUMP-2) performance, ultimately causing inconsistent flow into the vaporizer and analyzer. Under optimal analysis conditions, the pressure is near ambient at PI-1. A decrease in pressure at PI-2 indicates upstream vacuum conditions or worn peristaltic pump tubing at PUMP-2. An increase in pressure at PI-2 indicates clogging downstream, which can occur as particulate loading within F-2, or as mineral precipitation within the capillary or vaporizer. The pressure at PI-2 generally varied between 200 kPa and 400 kPa, depending on the injection air pressure and the precipitate levels within the vaporizer or capillary tubing. High-pressure vaporizer conditions allow sample to flow despite the inevitable accumulation of precipitation within the vaporizer, which enables the system to operate in balance for days or even weeks before it is necessary to clean the system components. However, over time, precipitate accumulation within the vaporizer can restrict the flow of air, water, or both; this typically requires a re-balancing of system flow conditions, but it can occasionally require removal and cleaning of impacted vaporizer components.

During analysis, intermittent reductions can occur in water vapor concentration within the vaporizer, which can produce a transient evaporation signal in the isotope data. Gkinis et al. (2010; 2011) described sample flow inconsistencies at their CFA flash vaporizer that cause extreme outliers in isotope data, though the cause of the fluctuations was unclear. We observe similar fluctuations, and the pressure sensor data provide insight into their cause. We find that the most common causes of such

https://doi.org/10.5194/egusphere-2022-60
Preprint. Discussion started: 25 April 2022

variations are microbubbles entering the vaporizer owing to particulate loading, which can cause poor debubbler performance and can also cause blockages to form within small tubing fittings. Microbubbles that remain suspended in the fluid stream after the debubbler cause volumetric flow rate reductions at the vaporizer inlet. Blockages within fittings upstream of PUMP-2 can cause extreme vacuum conditions before the pump (i.e., pressure observations associated with blockages were as low as -140 kPa before PUMP-2 instead of the typical ambient conditions); this can lead to the contamination of system tubing with small bubbles that also cause temporary flow reductions. To avoid these inconsistencies, we find that it is critical to routinely clean the debubbler membrane and to maintain ambient pressure at the PUMP-2 inlet by cleaning clogged filter screens or tubing fittings when indicated. Although data outliers could be systematically removed (as done in Gkinis et al., (2011)), occasional bubbles do not substantially impact the isotopic mean value of our ice core measurements and are retained here. We do exclude some reference-water calibration data, where bubble interruptions are most frequent due to limited operator oversight during automated reference water measurements. Calibration measurement criteria are discussed in Section 2.6, below.

In addition to monitoring pressure evolution across the system, we can also observe the quality of vapor at the CRDS analyzer via characteristic patterns that arise in the instantaneous analyzer output. Specific patterns in water vapor concentration and $\delta^{18}O$ that emerge from incomplete vaporization or unstable flow into the vaporizer are shown in Fig. 3. Incomplete vaporization is indicated by anticorrelated changes in water vapor concentration and $\delta^{18}O$. Anticorrelated patterns in water vapor concentration and $\delta^{18}O$ are common when there is insufficient backpressure on PUMP-2; large-amplitude (>70 kPa) pressure fluctuations from the peristaltic pump can cause pulsating flow into the vaporizer that alternates between overwhelming and undersupplying water to the vaporizer. The resulting patterns have a large amplitude (up to 10,000 ppm for water vapor, and several per mil for $\delta^{18}O$) and a frequency that mirrors that of the peristaltic pump (e.g., Fig. 3a). The apparent fractionation that occurs during these vaporization conditions leads to very poor calibration values for $\Delta^{17}O$, causing errors of 10s to 100s of per meg. If there is sufficient backpressure at PUMP-2, the pressure readings at PI-2 are typically <40 kPa. We attribute small fluctuations in $\delta^{18}O$ that are anticorrelated with water vapor concentration to the incomplete vaporization of individual droplets (e.g., Fig. 3b). Because flow inconsistencies are associated with isotope fractionation, we routinely tune the system to maintain steady pressure readings at the vaporizer inlet; this is done by adjusting the peristaltic pump rate, replacing filter screens at F-1 or F-2, adjusting FV-1, replacing peristaltic pump tubing, replacing or cleaning the capillary tube, or cleaning the vaporizer. Vapor concentration data that is typical of a well-maintained CFA system are shown in Fig. 3d.

2.5 Measuring $\Delta^{17}O$ by CFA-CRDS in ice core samples

The CFA system was configured to automatically measure an alternating sequence of three local reference waters over a period of approximately seven weeks; reference waters included SW2, CW, and SPS2, as shown in Table 1 and indicated in Fig. 2. The system was tuned and maintained as described above. Between reference measurements, an operator prepared and measured a slice of ice core.

https://doi.org/10.5194/egusphere-2022-60
Preprint. Discussion started: 25 April 2022

We cut an 87.5-cm ice core sample, from ~92 m depth beneath the surface at Summit, Greenland, into nine 26-mm square slices to prepare them for continuous analysis. After preparing these nine CFA sticks, a tenth section of core was cut into 63 discrete depth intervals. Discrete ice samples were melted in sealed polyethylene sample bottles in a refrigerator at 4° C. We measured the 87.5-cm section of ice ten times: the nine replicate slices were measured by the CFA-CRDS configuration described above, and the tenth measurement was made by discrete injection of 63 melt samples from the core using the commercially available vaporizer unit (Picarro p/n A0211) and automated injections as in Schauer et al. (2016). The resolution of the discretely measured ice is 1.39 cm.

For all CFA measurements, we used manual observations of the core height to monitor the melt rate during analysis, then later assigned a high-resolution depth equivalent for each analysis time that is based on the value of $\delta^{18}O$ and the measured depth of discrete samples. Previous work has monitored core depth with electronic distance meters (e.g., Bigler et al., 2011; Jones et al., 2017), and such measurements are critical for depth registration for routine CFA measurement campaigns. Here, we forego electronic depth registration and instead adjust initial depth estimates for each core section by aligning the seasonal cycle of $\delta^{18}O$ for all core samples. Summit, Greenland has a modern annual accumulation rate of 24 ± 5 cm (ice equivalent) per year (Meese et al., 1994; Dibb and Fahnestock, 2004; Hawley et al., 2008; 2021), and we expect to see two to three years represented by the core sample that we measured in replicate (Hastings et al., 2009). Assigning depths by aligning the $\delta^{18}O$ variations should largely eliminate depth-registration errors, since the strong seasonal $\delta^{18}O$ variations must be essentially identical in each replicate sample, and the signal to noise ratio for $\delta^{18}O$ is very high. We compressed the depth scale of each CFA record to maximize the cross-correlation of $\delta^{18}O$ ($0.93<R<0.99$) between the CFA measurements and the discrete measurements. We then assigned each CFA analysis time a depth equivalent based on the depth of the corresponding discrete $\delta^{18}O$ data. We note that the magnitude of the seasonal variations in $\delta^{18}O$ are somewhat compressed in the lower ~30 cm of this core sample, so the depth designations for this interval are likely a greater source of error than in the rest of the ice. Nevertheless, we are confident that our depth registration is precise to within a cm or better throughout the core.

2.6 Calibrating CFA-CRDS $\Delta^{17}O$ data

To calibrate our $\Delta^{17}O$ measurements, we create a two-point linear calibration curve for $\delta^{17}O$ and $\delta^{18}O$ from the nearest measurements of our internal reference waters, SW2 and SPS2; a third reference water (CW) is used as an independent verification of the calibration. The values of SW2, CW, and SPS2 have been measured independently and are normalized to the VSMOW-SLAP scale as in Schoenemann et al. (2013). Three-hour measurements of these alternating reference waters were made between measurements of the ice core sample. Because measurement conditions evolve over time due to particulate loading and mineral precipitation within the CFA components, there were periods of time during which the water vapor concentration was outside the ideal range or during which large bubbles or other flow inconsistencies degraded the quality of reference water data. We automatically reject calibration data that were generated from water vapor concentration beyond the targeted range (i.e., <20,000 or >50,000 ppm) or data with insufficient vaporizer operations, indicated by $\sigma_{\delta 18O} > 0.5$ ‰. We

https://doi.org/10.5194/egusphere-2022-60
Preprint. Discussion started: 25 April 2022

identify transitions from one reference water to the next in the data by the second derivative of δD, and assign known standard values based on the uncalibrated measurement values of δD. We include measurements of SW2 and SPS2 that contain at least 6000 s of analysis time and we trim 360 s of data from the beginning and end of each measurement interval to avoid memory effects. The mean and standard deviation of the analysis time for calibration standard data is 9350 s ± 660 s. For the measurement interval reported in this study, we use a calibration curve made from 47 continuous, 3-hour measurements of SW2 and 40 continuous, 3-hour measurements of SPS2. All analyzes include measurements for $\delta^{17}O$, $\delta^{18}O$, and δD. Calculations of *d* and $\Delta^{17}O$ were obtained from the calibrated δ values as given in equations [1] and [2], respectively.

2.7 Processing CFA-CRDS $\Delta^{17}O$ data

After assigning approximate depth values and calibrating the raw ~1-Hz data, we discretize the CFA-CRDS data by binning the calibrated data into prescribed depth intervals and averaging across the entire interval. This enables quantitative comparison between the continuous CFA-CRDS timeseries and the discrete CRDS measurements. Small differences in the instantaneous melt rate cause some variability in the data-averaging duration for each reported measurement; the typical instantaneous melt rate was ~0.3 cm/min, but rates ranged from ~0.1 cm/min to ~0.4 cm/min during analysis. We report our CFA-CRDS measurements with 1.39-cm resolution to match the resolution of our discrete CRDS measurements. We also explore the effects of depth resolutions that range from 0.5 cm to ~40 cm, given that increasing the averaging window of the ~1-Hz spectroscopic measurements reduces instrumental noise (e.g., Werle et al., 1993; Gkinis et al., 2010; 2011; Steig et al., 2014; 2021; Schauer et al., 2016; Jones et al., 2017).

3 Results and analysis

Our measurements show approximately two years of isotope observations, as expected for a Greenland ice core from the depth we analyzed (discussed in Section 2.5). The seasonal cycle of $\delta^{18}O$ is shown in Fig. 4. The high correlations ($r > 0.93$) among the nine different replicate $\delta^{18}O$ profiles confirm that our depth assignments are appropriate for this application. We estimate that our depth assignments are accurate to <7 mm throughout the core. This allows us to compare CFA-CRDS measurements of $\Delta^{17}O$ at the ~cm scale, appreciably finer resolution than has previously been reported.

3.1 Seasonal $\Delta^{17}O$ variations in replicated CFA and discrete measurements

We present the mean value and standard error of all replicate measurements in Fig. 4 with 1.39-cm averaging (representing approximately 270 s of data per interval); Figure 4 also shows the discrete CRDS measurements with the root mean square error of the corresponding discrete reference water measurements. The mean of all CFA-CRDS measurements is well correlated with the discrete measurements ($r = 0.52$), especially in the upper 50 cm of the core ($r = 0.70$).

https://doi.org/10.5194/egusphere-2022-60
Preprint. Discussion started: 25 April 2022

Both the CFA-CRDS measurements and the discrete CRDS data set show clear seasonal $\Delta^{17}O$ variations. Coarsening the depth resolution for the discretized CFA-CRDS dataset improves the correlation of seasonal $\Delta^{17}O$ information because it increases the effective averaging time for each measurement interval; averaging multiple replicate datasets (as in Fig. 4) should similarly improve the results. We explore the relationship between the correlation of CFA-CRDS data to discrete CRDS data and the quantity and duration of CFA-CRDS measurements included in the analysis. Figure 5 illustrates the impact of longer analysis times on the correlation of seasonal information. Figure 5 demonstrates that the correlation between CFA-CRDS seasonality and discrete CRDS seasonality improves as more measurement data is included in the average – both by averaging multiple CFA timeseries and by coarsening the depth resolution. All depth discretization schemes identified in Fig. 5 can sufficiently resolve the seasonal cycle of $\Delta^{17}O$ in our analysis. While combining multiple CFA-CRDS measurements does improve the $\Delta^{17}O$ signal, making replicate measurements of most ice core samples is impractical owing to limited sample availability. Additionally, the isochronal lines in Fig. 5 suggest that high-frequency information is most reliably detected by using longer averaging times within a single dataset and not by stacking multiple measurements; longer averaging times are generally achieved by melting the ice more slowly.

3.2 Error attribution for CFA-CRDS $\Delta^{17}O$ measurements

In addition to possible depth alignment errors, sources of variability in our CFA-CRDS measurements include high-frequency instrumental noise, calibration error, and noise generated by mixing within the CFA system. High-frequency, high-amplitude noise (~1 ‰) in the raw CRDS data is inherent to the instrument and can cause large aberrations from the true value of $\Delta^{17}O$, especially over short averaging times; long averaging times (>1000 s) are typically used when measuring $\Delta^{17}O$ by CFA-CRDS to reduce the impact of this instrumental noise. Calibration errors in $\Delta^{17}O$ are caused by disproportionate drift in $\delta^{17}O$ and $\delta^{18}O$ between measurements of calibration standards and samples; this is a direct effect of oxygen isotope fractionation during vaporization. Despite efforts to monitor and minimize isotope fractionation during measurement, it is likely that calibration errors persist. Finally, CFA-CRDS measurement error for $\Delta^{17}O$ may result from mixing isotopically distinct waters during CFA processing.

Typical CRDS characterization studies have used repeated measurements of reference waters to identify measurement error. By measuring reference waters, it is possible to approximate the precision of the uncalibrated measurements by determining the effect of averaging time on the intrinsic noise of the measurement; it is also possible to quantify the variance of the calibrated, averaged data. Our replicate CFA-CRDS measurements provide an opportunity to interrogate the source of CFA-CRDS errors because we can separately analyze the variability internal to each timeseries (e.g., due to the seasonal cycle of $\Delta^{17}O$) and the variability between the mean values of the nine measurements.

To isolate the calibration error, we processed the data in two ways: first, by calibrating the data as described and reported above, and second, by removing the mean value of each calibrated CFA-CRDS dataset. We discretized the CFA-CRDS data

https://doi.org/10.5194/egusphere-2022-60
Preprint. Discussion started: 25 April 2022

to a series of depth-resolution schemes that ranged from 1.39 cm to 43.75 cm. We calculated the standard error for all measurement resolutions. The total error for the calibrated data is approximated by the black line in Fig. 6, which represents the mean of the standard error at every depth interval. The total span of the standard error across depth intervals is provided by the grey shaded region. Similarly, the blue shaded region shows the total span of the standard error for the datasets with the mean removed, and the blue line is the mean error. The region between the two solid lines is the fraction of the total error that can be attributed to calibration error. The results show that the total error is <10 per meg for all data. The total error is ~5 per meg at averaging times longer than ~3000 s, which corresponds to depth averages of ~15 cm. Figure 6 also shows that the internal error for the CFA-CRDS data is <2 per meg with similar averaging and that the total error is dominated by calibration error at long averaging times.

In addition to error attribution, these replicate datasets provide an opportunity to compare the measured CFA-CRDS variability of ice core samples with the theoretical variability determined by an Allan variance analysis. An Allan variance analysis can be used to identify the relationship between internal noise and integration time (Allan, 1966; Werle et al., 1993). For CRDS data, Allan variance analysis of reference water measurements is commonly used to approximate the measurement precision of the system (Gkinis et al., 2010; Steig et al., 2014). We determine the Allan deviation (square-root of the Allan variance) from a long continuous analysis (~8.5 hours) of the SW2 reference water that was made between the sixth and seventh CFA-CRDS measurements; the result is shown in Fig. 7. This calculation – based only on the reference waters – does not account for additional variability that may originate from the CFA measurement or calibration processes, so we are also interested in any differences between the Allan deviation and the standard deviation of our measurements. Therefore, we find the standard deviation $\sigma_{CFA\text{-}\Delta17O}$ among all nine calibrated and discretized CFA-CRDS datasets, averaged over integration windows that vary from 5 mm to 43.75 cm. We track the analysis time associated with each averaging interval and overlay the measured $\sigma_{CFA\text{-}\Delta17O}$ with corresponding mean integration time for each depth interval on Fig. 7a.

Figure 7a shows generally good agreement between $\sigma_{CFA\text{-}\Delta17O}$ and $\sigma_{Allan\text{-}\Delta17O}$ at integration times less than 400 s, but the $\sigma_{CFA\text{-}\Delta17O}$ data asymptotically approach a limit of 10 per meg at longer averaging times instead of following the trend predicted by the Allan variance analysis. To evaluate to what extent this mismatch between expected and observed σ can be attributed to calibration error, we repeat this analysis for the dataset with the mean-adjusted value. Figure 7b shows excellent agreement between $\sigma_{CFA\text{-}\Delta17O}$ and $\sigma_{Allan\text{-}\Delta17O}$ at all integration times when the calibration error is eliminated; this demonstrates that the drift in $\sigma_{CFA\text{-}\Delta17O}$ shown in Fig. 6a can be entirely attributed to calibration errors, and not to the CFA process directly. Figure 7 suggests that the precision of calibrated CFA-CRDS measurements is not limited by the CFA process – nor to limitations of the CRDS instrument – but rather by the quality of the calibration, which depends entirely on the consistency of calibration water measurements.

https://doi.org/10.5194/egusphere-2022-60
Preprint. Discussion started: 25 April 2022

4 Discussion and Conclusions

4.1 Comparison of CFA-CRDS $\Delta^{17}O$ measurements to other $\Delta^{17}O$ measurements from Greenland

Our work complements previous studies that have examined the seasonal cycle of $\Delta^{17}O$ in polar regions, and good agreement with earlier work validates our measurements. Consistent with previous measurements from Greenland, the $\Delta^{17}O$ signal in our data is anticorrelated with *d* and anticorrelated with the seasonal cycle in $\delta^{18}O$ (Landais et al., 2008). The measurements presented here were made from core that represents approximately two years of ice accumulation from the 1760s (Hastings et al., 2009). The measured magnitude (peak to trough) of the seasonal cycle in $\Delta^{17}O$ is ~45 per meg at 1.39 cm resolution in our data (Fig. 4), which is in excellent agreement with the magnitude of the seasonal cycle reported previously for Greenland. Specifically, Landais et al. (2012b) reported seasonal magnitudes of ~25 per meg from a shallow firn core at NEEM (in Northwest Greenland) that represented accumulation periods between 1962-1963 and between 2003-2005; when we coarsen our measurement resolution to 3.6 cm – which approximates the ~monthly (5-cm) measurement resolution in the NEEM core (detailed in Steen-Larsen et al., 2011) – the magnitude of the seasonal cycle in our data is ~30 per meg. Low errors between replicate values and the good agreement with previous studies strengthen confidence in the CFA-CRDS approach for high-resolution $\Delta^{17}O$.

Our results reinforce the use of the CFA-CRDS method for high-precision, high-resolution measurements of $\Delta^{17}O$ in ice cores. CFA-CRDS methods are valuable for detecting detail in $\Delta^{17}O$ variations in deep ice layers, for measuring $\Delta^{17}O$ in ice from sites with low accumulation rates, or for measuring $\Delta^{17}O$ in any glacial ice where high depth resolution is desired.

4.2 Addressing CFA-CRDS calibration errors in $\Delta^{17}O$

Our combined CFA-CRDS dataset (including nine independent CFA measurements) shows that, like dual-inlet IRMS operations, stacking the CFA-CRDS data effectively averages over calibration inconsistencies; the results are comparable to highly resolved discrete CRDS or IRMS measurements. However, it is generally impractical to replicate measurements in this way because sample volume is limited, and it is therefore critical that CFA-CRDS methods for $\Delta^{17}O$ are designed to minimize calibration error for individual measurements.

In this study, we have minimized calibration errors of individual CFA-CRDS measurements by closely monitoring sample injection conditions at the custom vaporizer. We also systematically reject all calibration data that does not meet basic criteria for variability and water vapor concentration. Nevertheless, CFA-CRDS calibration may be affected by the differences in vaporization conditions between the sample and reference water. Because small changes in flow conditions within the vaporizer result from particulate loading and mineral precipitation over time, the best calibration is achieved when reference standards are measured immediately before or after the sample melt. It is therefore important to ensure balanced vaporizer conditions prior to making measurements of an ice core. We also observe that pressure balance at the vaporizer was easiest to

https://doi.org/10.5194/egusphere-2022-60
Preprint. Discussion started: 25 April 2022

maintain, and the calibration was therefore more consistent, when the vaporizer had recently been cleaned; cleaning the vaporizer eliminates mineral precipitation that affects air and water flow within the vaporizer.

Large errors in $\Delta^{17}O$ were occasionally observed during the analysis of the South Pole ice core (SPC14); Steig et al. (2021) attributed these errors to calibration differences and performed a correction by shifting the mean value of their measurements based on the offset identified by a calibrated reference water measurement. Our analysis supports the attribution of the SPC14 errors to calibration issues and additionally supports their application of a calibration adjustment. However, it would be ideal to identify and eliminate sources of calibration error so that such an adjustment is not necessary. In our vaporizer, it is likely that microphysical, precipitation-based changes to the geometry of the vaporizer chamber lead to incomplete vaporization and impact the calibration as precipitation builds up within the vaporizer over time. When there is clear evidence of inconsistent vaporization (as in Fig. 3), we observe large calibration errors in $\Delta^{17}O$ by this method (10s to 100s of per meg). Such issues likely also influence the vaporization process in other CFA systems, though they will not be readily detected in measurements of $\delta^{18}O$ or δD.

5 Summary

We measured $\Delta^{17}O$ in nine replicate ice core samples using a continuous flow analysis (CFA) system combined with a cavity-ring down laser spectroscopy (CRDS) instrument. We measured a tenth replicate sample by discrete CRDS methods. We show that extending the duration of ~1-Hz CFA-CRDS measurements that are included in an average – either by measuring at slower rates or by producing and combining multiple measurements – improves the $\Delta^{17}O$ signal, and that slower measurement rates lead to the highest fidelity measurements. We also demonstrate that the CFA process itself is not an important source of error in these CFA-CRDS measurements; rather, the total error (~5 per meg) is dominated by calibration uncertainties.

Our data show that CRDS methods can reliably capture seasonal information; we measured seasonal fluctuations of ~45 per meg in $\Delta^{17}O$ from an ice core representing the preindustrial period at Summit, Greenland. Our work highlights the potential for CFA-CRDS measurements to be applied to ice core measurements where high-resolution $\Delta^{17}O$ information is desired.

https://doi.org/10.5194/egusphere-2022-60
Preprint. Discussion started: 25 April 2022

References

Allan, D.: Statistics of atomic frequency standards, Proc IEEE, 52, 221, 1966.

Angert, A., Cappa, C. D., & DePaolo, D. J.: Kinetic 17O effects in the hydrologic cycle: Indirect evidence and implications. Geochimica et Cosmochimica Acta, 68 , 3487–3495. https://doi.org/10.1016/j.gca.2004.02.010, 2004.

Aron, P. G., Levin, N. E., Beverly, E. J., Huth, T. E., Passey, B. H., Pelletier, E. M., Poulsen, C. J., Winkelstern, I. Z., and Yarian, D. A.: Triple oxygen isotopes in the water cycle, Chemical Geology, 565, 120026. https://doi.org/10.1016/j.chemgeo.2020.120026, 2021.

Barkan, E., and Luz, B.: High precision measurements of17O/16O and18O/16O ratios in H2O, Rapid Commun. in Mass Spectrom., 19, 3737–3742, https://doi.org/10.1002/rcm.2250, 2005.

Barkan, E., and Luz, B.: Diffusivity fractionations of H216O/H217O and H216O/H218O in air and their implications for isotope hydrology. Rapid Commun. in Mass Spectrom., 21, 2999–3005, https://doi.org/10.1002/rcm.3180, 2007.

Berman, E.S.F., Levin, N.E., Landais, A., Li, S., and Owano, T: Measurement of δ18O, δ17O, and 17O-excess in water by Off-Axis Integrated Cavity Output Spectroscopy and Isotope Ratio Mass Spectrometry. Analytical Chemistry, 85, 10392-10398, https://doi.org/10.1021/ac402366t, 2013.

Bigler, M., Svensson, A., Kettner, E., Vallelonga, P., Nielsen, M. E., & Steffensen, J. P.: Optimization of High-Resolution Continuous Flow Analysis for Transient Climate Signals in Ice Cores, Environmental Science & Technology, 45, 4483–4489. https://doi.org/10.1021/es200118j, 2011.

Dibb, J.E. and Fahnestock, M.: Snow accumulation, surface height change, and firn densification at Summit, Greenland: Insights from 2 years of in situ observation, Journal of Geophysical Research, 109, 0148-0227, https://doi.org/10.1029/2003JD004300 , 2004.

Dansgaard, W.: Stable isotopes in precipitation, Tellus, 16, 436– 468, https://doi.org/10.1111/j.2153-3490.1964.tb00181.x, 1964.

Emanuelsson, B. D., Baisden, W. T., Bertler, N. A. N., Keller, E. D., and Gkinis, V.: High-resolution continuous-flow analysis setup for water isotopic measurement from ice cores using laser spectroscopy, Atmospheric Measurement Techniques, 8, 2869–2883, https://doi.org/10.5194/amt-8-2869-2015, 2015.

Gkinis, V., Popp, T. J., Johnsen, S. J., and Blunier, T.: A continuous stream flash evaporator for the calibration of an IR cavity ring-down spectrometer for the isotopic analysis of water, Isotop. Environ. Health Stud., 46, 463–475, 2010.

Gkinis, V., Popp, T. J., Blunier, T., Bigler, M., Schüpbach, S., Kettner, E., and Johnsen, S. J.: Water isotopic ratios from a continuously melted ice core sample, Atmos. Meas. Tech., 4, 2531– 2542, doi:10.5194/amt-4-2531-2011, 2011.

Gkinis, V., Simonsen, S. B., Buchardt, S. L., White, J. W. C., and Vinther, B. M.: Water isotope diffusion rates from the NorthGRIP ice core for the last 16,000 years-Glaciological and paleoclimatic implications, Earth Planet. Sc. Lett., 405, 132–141, 2014.

https://doi.org/10.5194/egusphere-2022-60
Preprint. Discussion started: 25 April 2022

Hastings, M. G., Jarvis, J. C., and Steig, E. J.: Anthropogenic Impacts on Nitrogen Isotopes of Ice-Core Nitrate. Science, 324, 5932, 1288–1288, https://doi.org/10.1126/science.1170510, 2009.

Hawley, R. L., Morris, E. M., & McConnell, J. R.: Rapid techniques for determining annual accumulation applied at Summit, Greenland. Journal of Glaciology, 54, 839–845. https://doi.org/10.3189/002214308787779951, 2008.

Hawley, R. L., Neumann, T. A., Stevens, C. M., Brunt, K. M., and Sutterly, T. C.: Greenland Ice Sheet elevation change: Direct observation of process and attribution at summit, Geophysical Research Letters, 47, https://doi.org/10.1029/2020GL088864, 2020.

Iannone, R. Q., Romanini, D., Cattani, O., Meijer, H.A.J., and Kerstel, E.R.T.:Water isotope ratio (d2H and d18O) measurements in atmospheric moisture using an optical feedback cavity enhanced absorption laser spectrometer, J. Geophys. Res., 115, D10111, https://doi.org/10.1029/2009JD012895, 2010.

Jones, T. R., White, J. W. C., Steig, E. J., Vaughn, B. H., Morris, V., Gkinis, V., Markle, B. R., and Schoenemann, S. W.: Improved methodologies for continuous-flow analysis of stable water isotopes in ice cores, Atmospheric Measurement Techniques, *10* 617–632, https://doi.org/10.5194/amt-10-617-2017, 2017.

Jones, T. R., Cuffey, K. M., White, J. W. C., Steig, E. J., Buizert, C., Markle, B. R., McConnell, J. R., and Sigl, M.: Water isotope diffusion in the WAIS Divide ice core during the Holocene and last glacial, Journal of Geophysical Research: Earth Surface, 122, 290–309, https://doi.org/10.1002/2016JF003938, 2017b.

Jouzel, J. and Merlivat, L.: Deuterium and oxygen 18 in precipitation: Modeling of the isotopic effects during snow formation, J. Geophys. Res.-Atmos., 89, 11749–11757, https://doi.org/10.1029/JD089iD07p11749, 1984.

Jouzel, J., Froehlich, K., and Schotterer, U.: Deuterium and oxygen-18 in present-day precipitation: Data and modelling, Hydrological Sciences Journal, 42, 747–763, https://doi.org/10.1080/02626669709492070, 1997.

Kahle, E. C., Holme, C., Jones, T. R., Gkinis, V., and Steig, E. J.: A Generalized Approach to Estimating Diffusion Length of Stable Water Isotopes From Ice-Core Data, Journal of Geophysical Research: Earth Surface, 123, 2377–2391. https://doi.org/10.1029/2018JF004764, 2018.

Kahle, E. C., Steig, E. J., Jones, T. R., Fudge, T. J., Koutnik, M. R., Morris, V. A., Vaughn, B. H., Schauer, A. J., Stevens, C. M., Conway, H., Waddington, E. D., Buizert, C., Epifanio, J., and White, J. W. C.: Reconstruction of Temperature, Accumulation Rate, and Layer Thinning From an Ice Core at South Pole, Using a Statistical Inverse Method, Journal of Geophysical Research: Atmospheres, 126, https://doi.org/10.1029/2020JD033300, 2021.

Kerstel, E. R. T., van Trigt, R., Dam, N., Reuss, J., and Meijer, H. A. J.: Simultaneous determination of the 2H / 1H, 17O / 16O and 18O / 16O isotope abundance ratios in water by means of laser spectrometry, Anal. Chem., 71, 5297–5303, 1999.

Landais, A., Barkan, E., and Luz, B.: Record of δ^{18}O and ^{17}O-excess in ice from Vostok Antarctica during the last 150,000 years, Geophys. Res. Lett., 35, 2, L02709, doi: 10.1029/2007GL032096, 2008.

https://doi.org/10.5194/egusphere-2022-60
Preprint. Discussion started: 25 April 2022

Landais, A., Ekaykin, A., Barkan, E., Winkler, R., and Luz, B.: Seasonal Variations of ^{17} O-Excess and d-Excess in Snow Precipitation at Vostok Station, East Antarctica, J. Glaciol., 58 , 210, 725–733, https://doi.org/10.3189/2012JoG11J237, 2012.

Landais, A., Steen-Larsen, H. C., Guillevic, M., Masson-Delmotte, V., Vinther, B., and Winkler, R.: Triple isotopic composition of oxygen in surface snow and water vapor at NEEM (Greenland), Geochimica et Cosmochimica Acta, 77, 304–316, https://doi.org/10.1016/j.gca.2011.11.022, 2012b.

Luz, B., & Barkan, E.: Variations of 17O/16O and 18O/16O in meteoric waters, Geochimica et Cosmochimica Acta, 74, 6276–6286, https://doi.org/10.1016/j.gca.2010.08.016, 2010.

Merlivat, L., and Jouzel, J.: Global climatic interpretation of the deuterium-oxygen 18 relationship for precipitation, Journal of Geophysical Research, 84, 5029, https://doi.org/10.1029/JC084iC08p05029, 1979.

Meese, D. A., Gow, A. J., Grootes, P., Stuiver, M., Mayewski, P. A., Zielinski, G. A., Ram, M., Taylor, K. C., & Waddington, E. D.: The Accumulation Record from the GISP2 Core as an Indicator of Climate Change Throughout the Holocene, Science, 266, 1680–1682, https://doi.org/10.1126/science.266.5191.1680, 1994.

Schauer, A.J., Schoenemann, S.W., and Steig, E.J.: Routine High-Precision Analysis of Triple Water-Isotope Ratios Using Cavity Ring-down Spectroscopy, Rapid Commun. Mass Spectrom., 30, 18, 2059-2069, 2016.

Schoenemann, S.W., Schauer, A.J., and Steig, E.J.: Measurement of SLAP2 and GISP δ17O and proposed VSMOW-SLAP normalization for δ17O and 17Oexcess, Rapid Commun. Mass Spectrom., 27, 582, 2013.

Schoenemann, S. W., Steig, E. J., Ding, Q., Markle, B. R., and Schauer, A. J.: Triple water-isotopologue record from WAIS Divide, Antarctica: Controls on glacial-interglacial changes in ^{17} O $_{excess}$ of precipitation: WAIS LGM-Holocene 17Oexcess Record, Journal of Geophysical Research: Atmospheres, 119, 14, 8741–8763, https://doi.org/10.1002/2014JD021770, 2014.

Schoenemann, S. W., and Steig, E. J.: Seasonal and spatial variations of ^{17} O $_{excess}$ and d_{excess} in Antarctic precipitation: Insights from an intermediate complexity isotope model, Journal of Geophysical Research: Atmospheres, 121, https://doi.org/10.1002/2016JD025117, 2016.

Steen-Larsen, H. C., Masson-Delmotte, V., Sjolte, J., Johnsen, S. J., Vinther, B. M., Bréon, F.-M., Clausen, H. B., Dahl-Jensen, D., Falourd, S., Fettweis, X., Gallée, H., Jouzel, J., Kageyama, M., Lerche, H., Minster, B., Picard, G., Punge, H. J., Risi, C., Salas, D., Schwander, J., Steffen, K., Sveinbjörnsdóttir, A. E., Svensson, A., and White, J.: Understanding the Climatic Signal in the Water Stable Isotope Records from the NEEM Shallow Firn/Ice Cores in Northwest Greenland., J. Geophys. Res., 116, D6, D06108, https://doi.org/10.1029/2010JD014311, 2011.

Steen-Larsen, H. C., Masson-Delmotte, V., Hirabayashi, M., Winkler, R., Satow, K., Prié, F., Bayou, N., Brun, E., Cuffey, K. M., Dahl-Jensen, D., Dumont, M., Guillevic, M., Kipfstuhl, S., Landais, A., Popp, T., Risi, C., Steffen, K., Stenni, B., & Sveinbjörnsdottír, A. E.: What controls the isotopic composition of Greenland surface snow? Climate of the Past, 10, 377–392. https://doi.org/10.5194/cp-10-377-2014, 2014.

https://doi.org/10.5194/egusphere-2022-60
Preprint. Discussion started: 25 April 2022

Steig, E.J., Gkinis, V., Schauer, A.J., Schoenemann, S.W., Samek, K., Hoffnagle, J., Dennis, K.J., and Tan, S.M.: Calibrated high-precision 17O-excess measurements using cavity ring-down spectroscopy with laser-current-tuned cavity resonance, Atmos. Meas. Tech., 7, 2421, 2014.

Steig, E. J., Jones, T. R., Schauer, A. J., Kahle, E. C., Morris, V. A., Vaughn, B. H., Davidge, L., and White, J. W. C.: Continuous-Flow Analysis of δ17O, δ18O, and δD of H2O on an Ice Core from the South Pole, Frontiers in Earth Science, 9, 640292, https://doi.org/10.3389/feart.2021.640292, 2021.

Tian, C., Wang, L., and Novick, K. A.: Water vapor δ2H, δ18O and δ17O measurements using an off-axis integrated cavity output spectrometer – sensitivity to water vapor concentration, delta value and averaging-time. Rapid Communications in Mass Spectrometry, 30, 2077–2086, https://doi.org/10.1002/rcm.7714, 2016.

Uemura, R., Barkan, E., Abe, O., and Luz, B.: Triple isotope composition of oxygen in atmospheric water vapor: the ^{17}O-excess of water vapor, Geophysical Research Letters, 37, L04402, https://doi.org/10.1029/2009GL041960, 2010.

Werle, P., Miicke, R., & Slemr, F.: The limits of signal averaging in atmospheric trace-gas monitoring by tunable diode-laser absorption spectroscopy (TDLAS). Applied Physics B Photophysics and Laser Chemistry, 57(2), 131–139. https://doi.org/10.1007/BF00425997, 1993.

https://doi.org/10.5194/egusphere-2022-60
Preprint. Discussion started: 25 April 2022

Figures and Tables

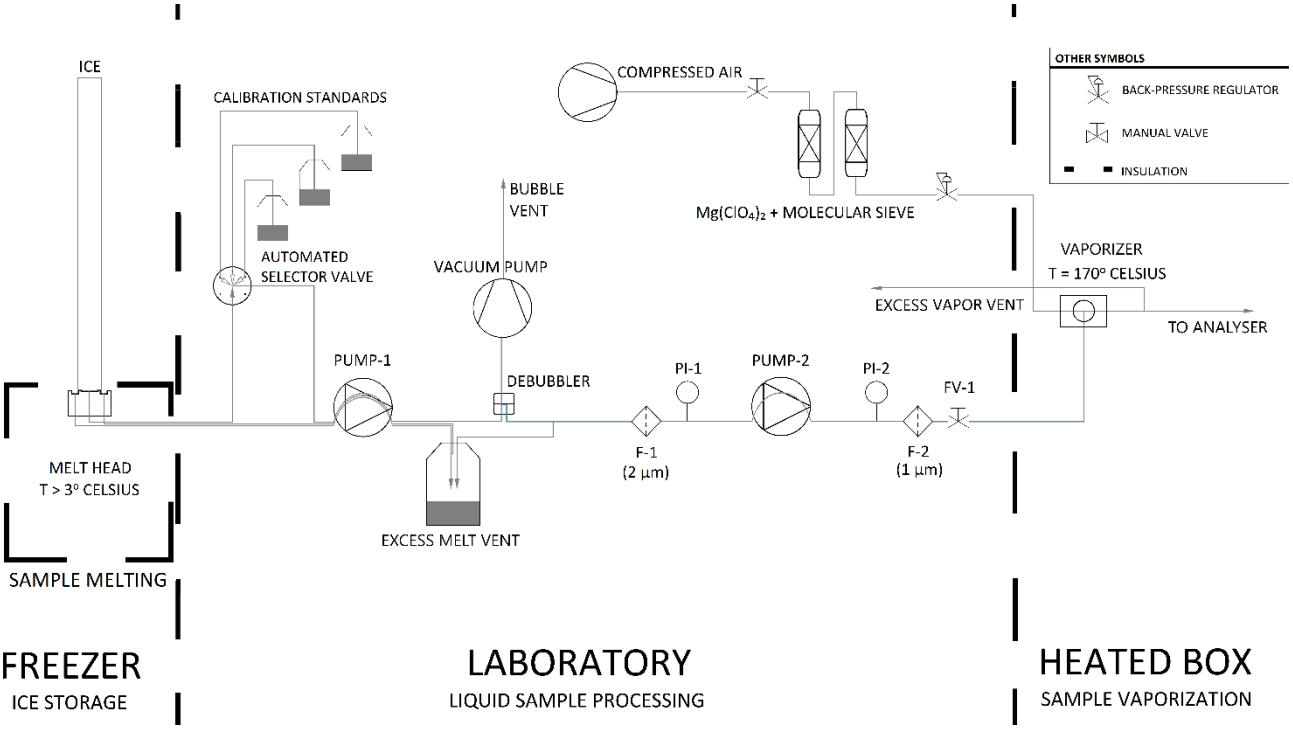

525 **Figure 1: Process flow diagram for CFA system. Thick dashed lines indicate transitions between temperature-controlled process spaces. Note that F-1 and F-2 are filters, PI-1 and PI-2 are pressure sensors, and FV-1 is a flow valve.**

https://doi.org/10.5194/egusphere-2022-60
Preprint. Discussion started: 25 April 2022

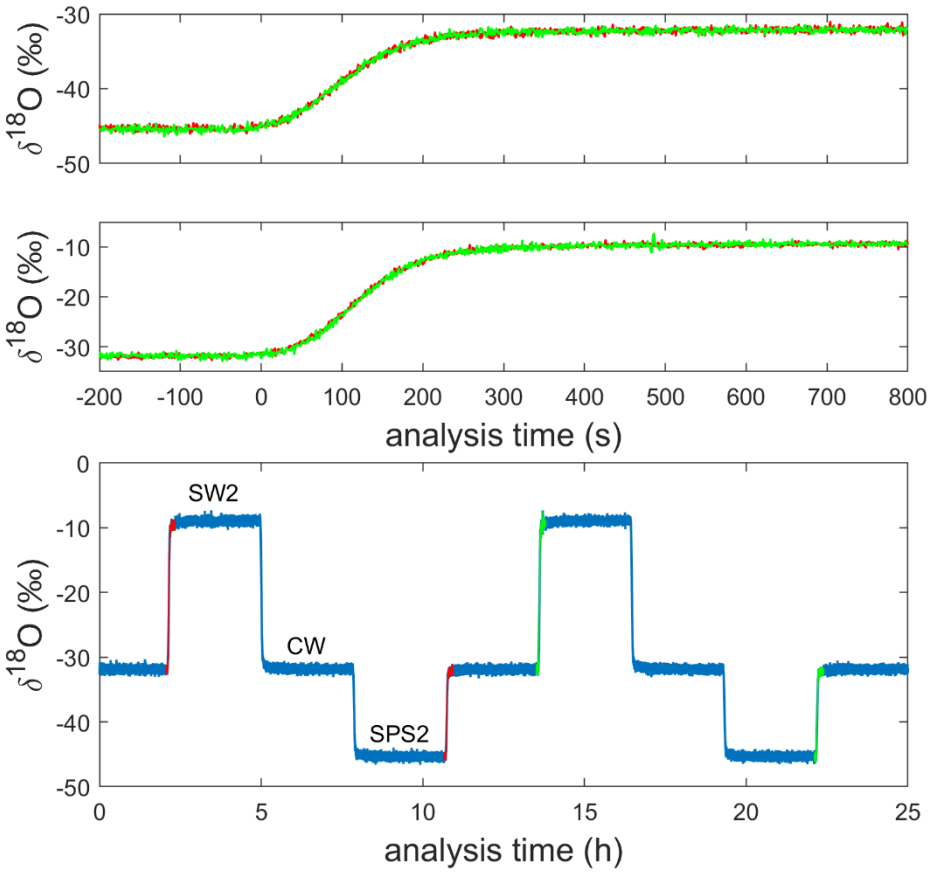

Figure 2: Uncalibrated, 1-Hz measurements of $\delta^{18}O$ for the alternating sequence of reference waters during a full analysis day (bottom). The 200 s preceding and 800 s following four reference water transitions are shown in the other panels; two transitions from SPS2 to CW are stacked in the top panel and two transitions from CW to SW2 are stacked in the middle panel.

https://doi.org/10.5194/egusphere-2022-60
Preprint. Discussion started: 25 April 2022

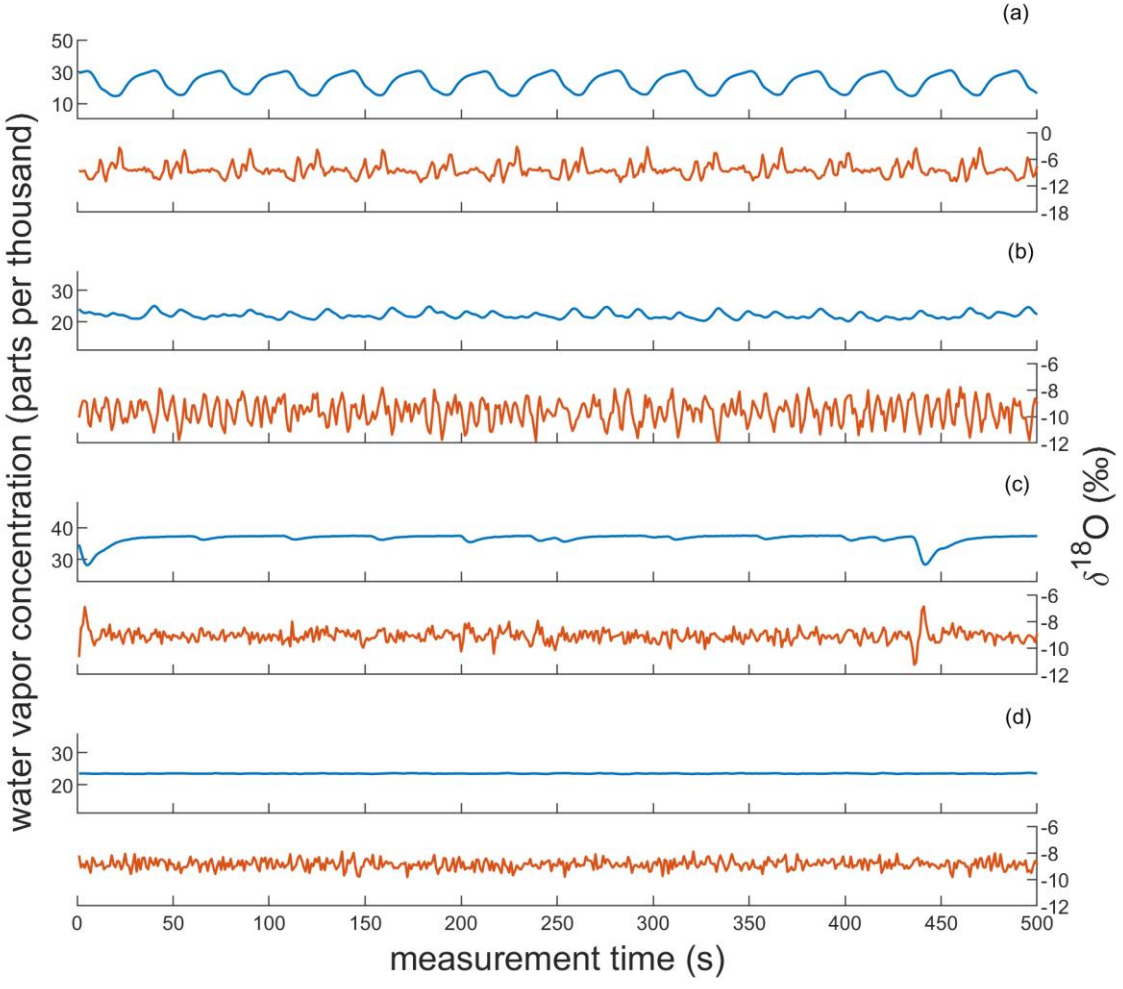

Figure 3: Observations of vapor quality as real-time indicators of vaporizer performance. Each subplot shows corresponding observations of water vapor concentration and $\delta^{18}O$ of SW2, reported parts per thousand and per mil, respectively. (A) and (B) show observations indicative of imbalanced vaporizer conditions for large and small pressure imbalances, respectively. (C) and (D) show observations indicative of acceptable vaporizer performance. Though both include low-variability observations of $\delta^{18}O$ (σ <0.3 ‰) and of water vapor concentration, (C) also includes microbubble interruptions at the vaporizer (e.g., at 5 and 440 s). (D) indicates optimal vaporizer performance. Note that the vertical scaling of (A) is different from the other panels.

https://doi.org/10.5194/egusphere-2022-60
Preprint. Discussion started: 25 April 2022

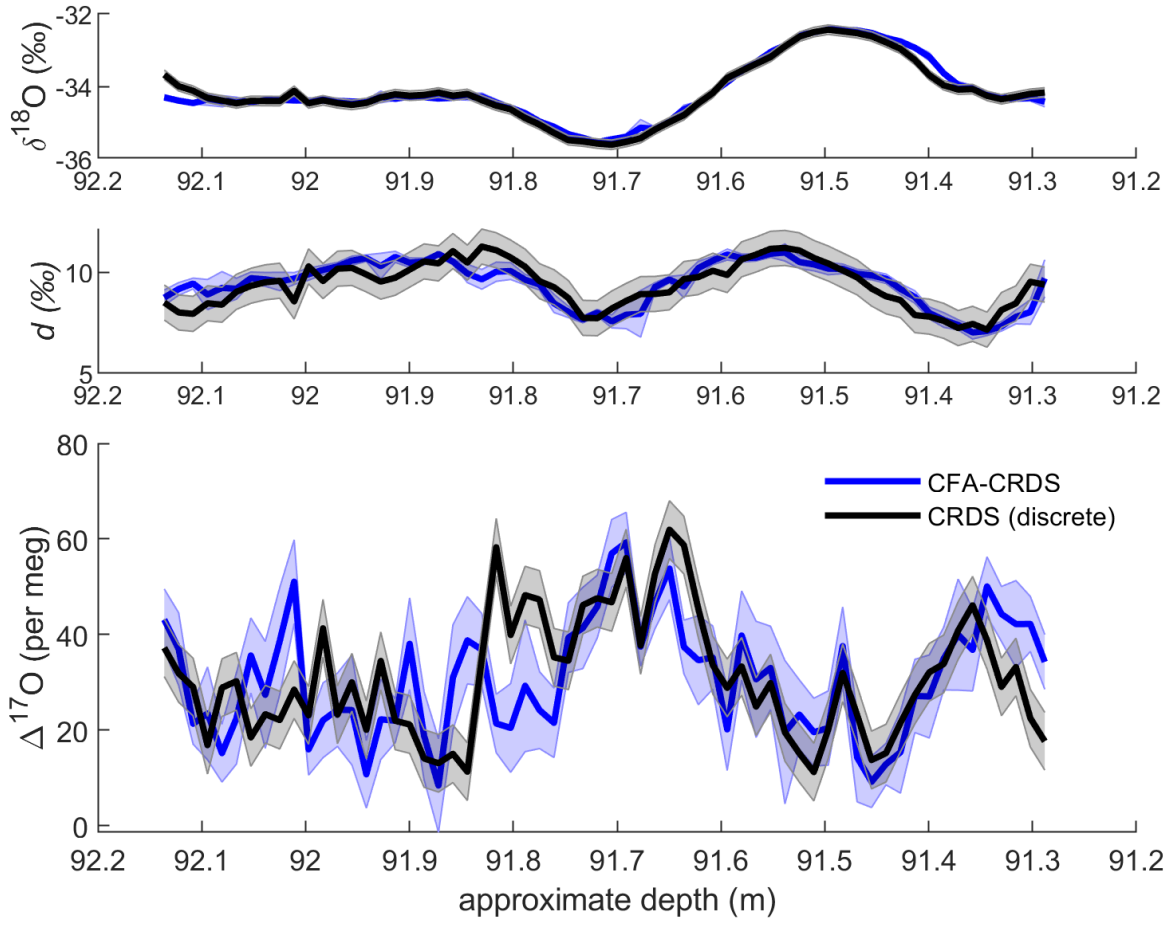

Figure 4: Comparison of discrete CRDS ice core measurements (black) with calibrated CFA-CRDS data averaged over 1.39-cm intervals (blue). Corresponding $\delta^{18}O$ and *d* data are shown for seasonal context. Discrete CRDS measurements are shown with the root mean square error of corresponding reference water measurements (grey shading), and CFA-CRDS measurements are shown as the mean of nine measurements with the standard error (blue shading).

https://doi.org/10.5194/egusphere-2022-60
Preprint. Discussion started: 25 April 2022

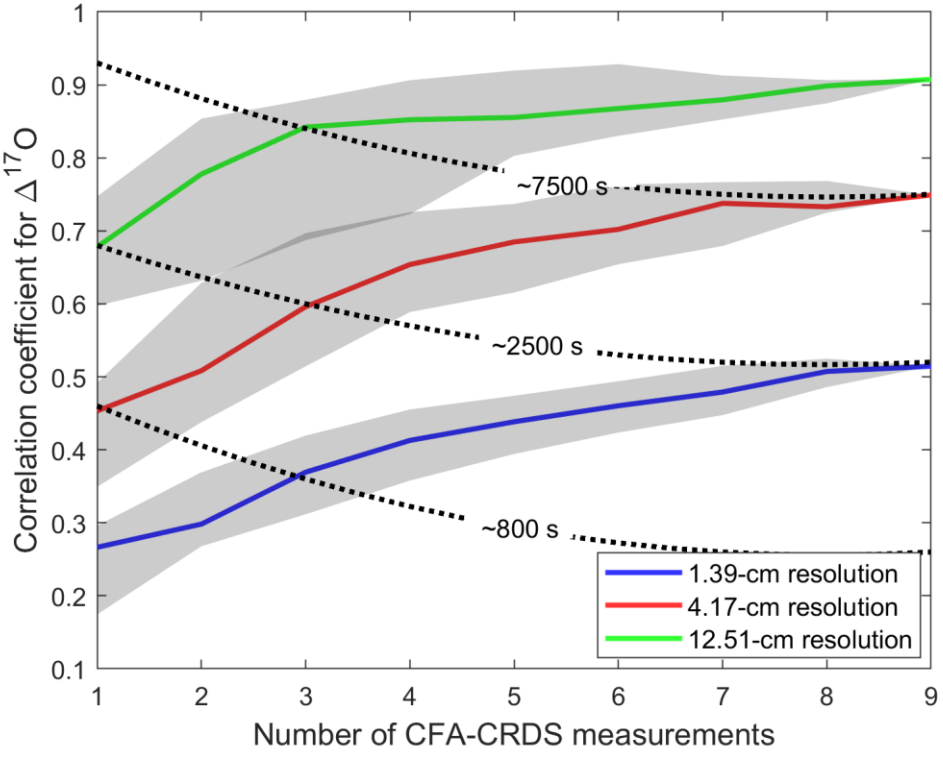

Figure 5: Correlation between discrete $\Delta^{17}O$ measurements and CFA measurements. The x-axis shows the number of replicate measurements that were combined by averaging before comparison with the discrete measurements. The solid lines show the median correlation coefficient for all dataset permutations; the shaded regions are constrained by the lower and upper quartiles for each depth resolution scheme. The dotted lines approximate isochronal surfaces, where approximately equal durations of CRDS raw data are included in the CFA-CRDS dataset.

https://doi.org/10.5194/egusphere-2022-60
Preprint. Discussion started: 25 April 2022

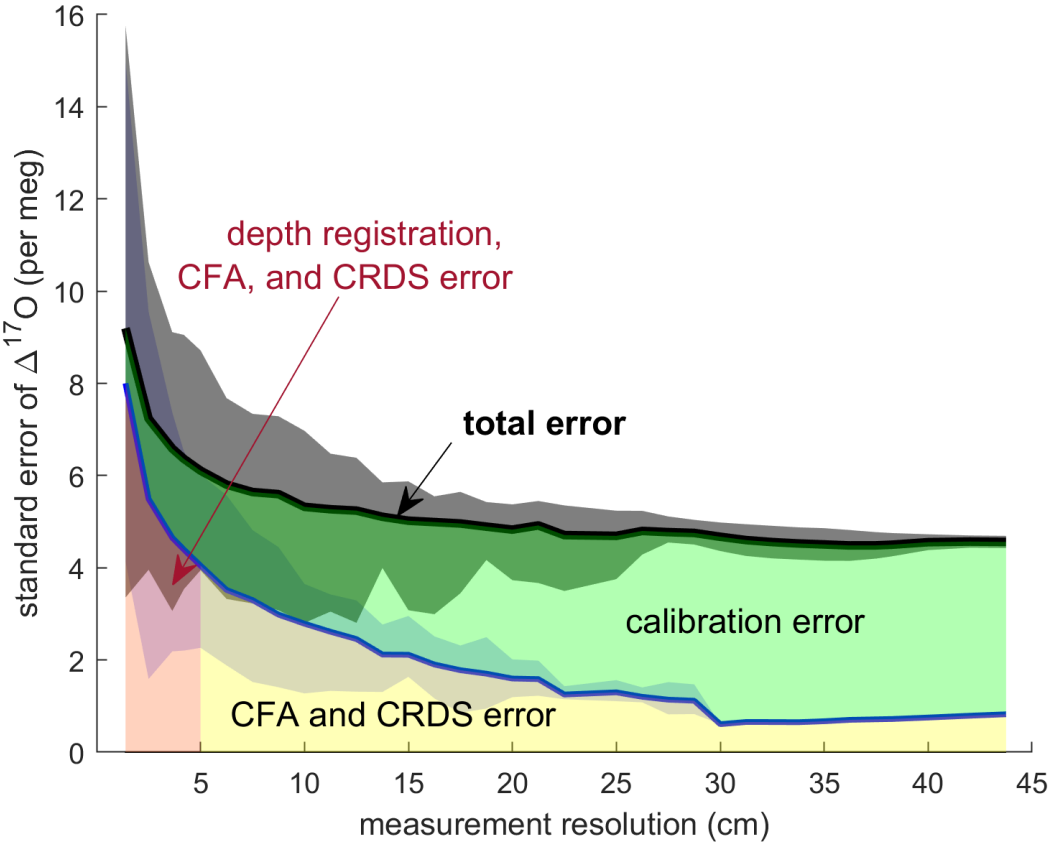

Figure 6: Standard error of all replicate CFA measurements by measurement integration depth. The black line shows the mean of the standard error as calculated for each depth interval; the shaded area indicates the minimum and maximum values of the standard error across all depth intervals. The blue line shows the relationship between the standard error in mean-shifted values and the measurement resolution. The area beneath the total error line is highlighted to indicate error attribution.

https://doi.org/10.5194/egusphere-2022-60
Preprint. Discussion started: 25 April 2022

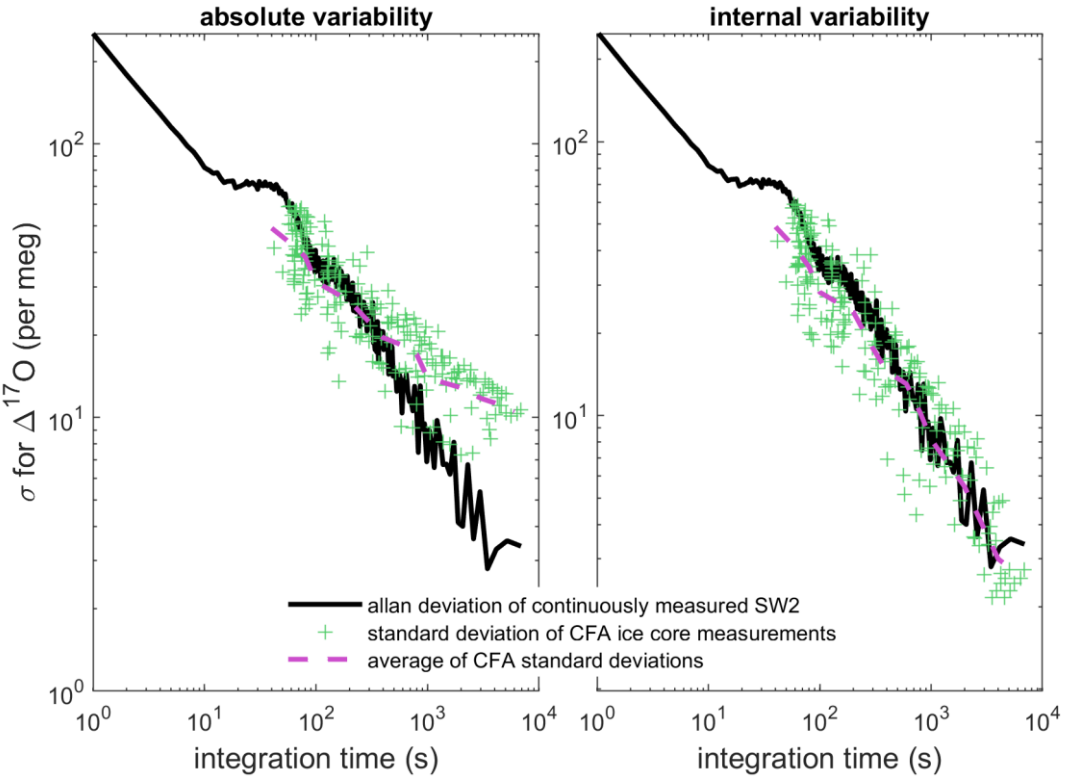

Figure 7: Comparison of Allan deviation of continuous reference water measurements and standard deviation of nine duplicate CFA ice core measurements. In both left and right images, the Allan deviation line (black) for a long measurement of SW2 is overlain by the standard deviation of the CFA-CRDS ice core measurements (green) and the mean of the standard deviations for each integration time (pink). The standard deviation on the left is calculated from calibrated replicate CFA-CRDS measurements and shows the absolute variability between CFA-CRDS replications. The standard deviation information in the right plot is calculated from the mean-shifted datasets so that only internal variability is considered in the analysis.

Reference water (origin location)	$\delta^{17}O$	$\delta^{18}O$	δD	*d*	$\Delta^{17}O$
	‰ vs. VSMOW				per meg vs. VSMOW
SW2 (Seattle)	-5.7107	-10.85	-77.96	8.84	33
CW (West Antarctica)	-17.8807	-33.64	-265.95	3.17	25
SPS2 (South Pole)	-25.1210	-47.07	-365.20	11.36	15

Table 1: Isotopic values of reference waters. SW2 is Seattle deionized tap water; CW is melt water from the WDC06A core (i.e., West Antarctic Ice Sheet precipitation), and SPS2 is South Pole snow. These three waters were normalized to the VSMOW-SLAP scale using other in-house reference waters that were analyzed against VSMOW, SLAP, and GISP (see Schoenemann et al., 2013).

https://doi.org/10.5194/egusphere-2022-60
Preprint. Discussion started: 25 April 2022

Data Availability

Measurement datasets generated and analyzed for this study are available from the corresponding author upon request.

Author Contribution

EJS, AJS, and LD conceived of the study. LD developed the measurement method, made the measurements, and completed the analysis with the support of AJS and EJS. All authors contributed to the manuscript.

Competing Interests

The authors declare that they have no conflict of interest.